



**HAL**  
open science

## Quaternary structural convergence and structural diversification of prion assemblies at the early replication stage

Angélique Igel-Egalon, Florent Laferrière, Mohammed Moudjou, Mathieu Merzach, Tina Knäpple, Laetitia Herzog, Fabienne Reine, Marie Doumic, Human Rezaei, Vincent Béringue

► **To cite this version:**

Angélique Igel-Egalon, Florent Laferrière, Mohammed Moudjou, Mathieu Merzach, Tina Knäpple, et al.. Quaternary structural convergence and structural diversification of prion assemblies at the early replication stage. 2023. hal-04264878

**HAL Id: hal-04264878**

**<https://hal.science/hal-04264878>**

Preprint submitted on 30 Oct 2023

**HAL** is a multi-disciplinary open access archive for the deposit and dissemination of scientific research documents, whether they are published or not. The documents may come from teaching and research institutions in France or abroad, or from public or private research centers.

L'archive ouverte pluridisciplinaire **HAL**, est destinée au dépôt et à la diffusion de documents scientifiques de niveau recherche, publiés ou non, émanant des établissements d'enseignement et de recherche français ou étrangers, des laboratoires publics ou privés.

1 **Quaternary structural convergence and structural diversification of prion**  
2 **assemblies at the early replication stage**

3  
4 Angélique Igel-Egalon<sup>1¶</sup>, Florent Laferrière<sup>1#¶</sup>, Mohammed Moudjou<sup>1¶</sup>, Mathieu Merzach<sup>1,2</sup>, Tina  
5 Knäpple<sup>1</sup>, Laetitia Herzog<sup>1</sup>, Fabienne Reine<sup>1</sup>, Marie Doumic<sup>2</sup>, Human Rezaei<sup>1\*</sup>, Vincent Béringue<sup>1\*</sup>

6  
7 <sup>1</sup>VIM, INRA, Université Paris-Saclay, 78350 Jouy-en-Josas, France

8 <sup>2</sup>INRIA, MAMBA, Université Paris VI, Paris, France

9 <sup>¶</sup>Equal contributors

10 <sup>#</sup>Current address: Institute of Neurodegenerative Diseases, CNRS UMR5293, University of Bordeaux,  
11 Bordeaux, France

12

13 \*Corresponding author and senior authorship: Vincent Béringue ([vincent.beringue@inra.fr](mailto:vincent.beringue@inra.fr)); Human  
14 Rezaei ([human.rezaei@inra.fr](mailto:human.rezaei@inra.fr)), MAP2, VIM, INRA- Domaine de Vilvert, 78352, Jouy-en Josas,  
15 France. Phone: (+33)1-34-65-26-00.

16

17

18

19

20

21 Acknowledgments

22 We thank the staff of the Animal facility (INRA-UEAR, Jouy-en-Josas) for animal care. This  
23 work was supported by grants from the Fondation pour la Recherche Médicale (Equipe FRM  
24 DEQ20150331689), the European Research Council (ERC Starting Grant SKIPPERAD,  
25 number 306321), and the Ile de France region (DIM MALINF).

26

## 27 **Abstract**

28 Aggregation of misfolded forms from host-encoded proteins is key to the pathogenesis of a  
29 number of neurodegenerative disorders, including prion diseases, Alzheimer's disease and  
30 Parkinson's disease. In prion diseases, the cellular prion protein PrP<sup>C</sup> can misfold into PrP<sup>Sc</sup>  
31 and auto-organize into conformationally distinct assemblies or strains. A plethora of  
32 observations reports the existence of PrP<sup>Sc</sup> structural heterogeneity within prion strains,  
33 suggesting the emergence and coevolution of structurally distinct PrP<sup>Sc</sup> assemblies during prion  
34 replication in controlled environment. Such PrP<sup>Sc</sup> diversification processes remain poorly  
35 understood. Although central to prion host-adaptation, structural diversification of PrP<sup>Sc</sup>  
36 assemblies is also a key issue for the formation of PrP conformers involved in neuronal injury.  
37 Here, we characterized the evolution of the PrP<sup>Sc</sup> quaternary structure during prion replication  
38 *in vivo* and *in bona fide* cell-free amplification assays. Regardless of the strain studied, the early  
39 replication stage conduced to the preferential formation of small PrP<sup>Sc</sup> oligomers, thus  
40 highlighting a quaternary structural convergence phenomenon. Their evolutionary kinetics  
41 revealed the existence of a PrP<sup>C</sup>-dependent secondary templating pathway in concert with a  
42 structural rearrangement. This secondary templating pathway provides, for the first time, a  
43 mechanistic explanation for prion structural diversification during replication, a key  
44 determinant for prion adaptation on further transmission, including to other host species. The  
45 uncovered processes are also key for a better understanding of the accumulation mechanisms  
46 of other misfolded assemblies believed to propagate by a prion-like process.

47

48 Keywords: prion / neurodegenerative disorders / polymerization / kinetics / diversification

49

## 50 **Introduction**

51 In terms of pathogenic mechanisms, the prion paradigm unifies a number of age-related,  
52 incurable neurodegenerative disorders that are caused by protein misfolding and aggregation  
53 [13,21,22,9]. These disorders include human and animal forms of prion diseases, Alzheimer's  
54 disease, Parkinson's disease and Huntington's disease. In principle, host-encoded monomeric  
55 proteins or peptides are converted into misfolded and aggregated assemblies, which serve as  
56 seeds or templates for further autocatalytic conversion. In prion diseases, the ubiquitously  
57 expressed, host-encoded prion protein PrP<sup>C</sup> is converted into a misfolded,  $\beta$ -sheet-rich  
58 conformer termed PrP<sup>Sc</sup> [39]. In susceptible host species and in laboratory rodent models, PrP<sup>Sc</sup>  
59 assemblies form stable, structurally distinct PrP<sup>Sc</sup> conformers [4,8,12,52], known as prion  
60 strains, and encode unique stereotypical biological phenotypes [45,47,48,5]. The strain-specific  
61 structural differences can be observed at the secondary structural level in terms of local  
62 structural variation but also at the quaternary level with strain-specific size distributions  
63 [44,49,47]. A large body of evidence supports the view for further structural diversity within  
64 specific prion populations and strains: i) some studies highlight the selection of prion substrains  
65 during the transmission of natural isolates [11,27,2] or experimental prion strains [29] with a  
66 species or transmission barrier, ii) size- or density-fractionation studies support the existence  
67 of a heterogeneous spectrum of PrP<sup>Sc</sup> assemblies with distinct tertiary/quaternary structures  
68 [24,44,49,23,50,6,7,41] and biological activity (templating activity and infectivity) [24,44,49],  
69 and iii) kinetic studies of prion pathogenesis suggest that the formation of neurotoxic PrP<sup>Sc</sup>  
70 species [46] occurs at the late stage of prion infection but that replicative PrP<sup>Sc</sup> assemblies are  
71 formed at earlier stages [42,43]. The prion replication process thus intrinsically allows the  
72 structural diversification of PrP<sup>Sc</sup> assemblies.

73 While the kinetic aspects of prion replication 'as a whole' have been comprehensively described  
74 by measuring infectivity or PrP<sup>Sc</sup> levels in the brain (see references [25,34] as examples), the

75 processes by which PrP<sup>Sc</sup> structural diversification and the formation of different  
76 subpopulations occur within a given strain remain undescribed and are not mechanistically  
77 supported in the actual framework of the prion paradigm. The autocatalytic conversion model  
78 proposed by Griffith in 1967 [17], the nucleated-polymerization model described by Lansbury  
79 and Caughey in 1995 [26] and other derived models (e.g., [30]) merely assume the existence of  
80 structurally homogenous assemblies that have absolutely identical propensity to replicate  
81 throughout disease progression. These mechanisms intrinsically reduce PrP<sup>Sc</sup> heterogeneity due  
82 to the best replicator selection process (35, 36). A recent high-resolution structural analysis of  
83 the N-terminal domain of the yeast prion Sup35 suggests that conformational fluctuations in  
84 natively disordered monomeric Sup35 are responsible for the stochastic, structural  
85 diversification of Sup35 aggregates [36]. This idea can be extrapolated to mammalian prion  
86 PrP to explain intrastrain structural diversification and strain mutation [12]. However, based on  
87 the best replicator selection concept [33,37,35], the aforementioned idea does not explain the  
88 coevolution of at least two structurally distinct PrP<sup>Sc</sup> subassemblies within the same  
89 environment [11,28].

90 To examine the molecular mechanisms of PrP<sup>Sc</sup> replication and structural diversification in  
91 depth, we explored, with sedimentation velocity (SV)-based methods, the early stage of prion  
92 conversion *in vivo* and in a cell-free system by protein misfolding cyclic amplification (PMCA).  
93 PMCA mimics *in vivo* prion replication with accelerated kinetics [40]. By using several prion  
94 strains as templates, we demonstrated that the early stage of prion replication invariably  
95 generates two subsets of assemblies, termed A<sub>i</sub> and B<sub>i</sub>, which differ in proportion, size and  
96 structure according to their specific infectivity. The analysis of their kinetics of formation  
97 during mb-PMCA combined with kinetic data assimilation revealed the existence of two  
98 sequential processes during prion replication. The first process corresponds to a quaternary  
99 structural convergence, as it tends to reduce the parental quaternary structure polydispersity to

100 generate mostly small-sized assemblies, namely  $A_i$ . The second process transforms the  $A_i$  into  
101 structurally different assemblies, namely,  $B_i$ , according to a secondary auto-catalytic pathway  
102 requiring PrP<sup>C</sup> and where  $B_i$  facilitates its own formation. Our findings provide, for the first  
103 time, mechanistic insights allowing the generation of structurally distinct assemblies during the  
104 prion replication process.

105

106

## 107 **Results**

### 108 **Small PrP<sup>Sc</sup> oligomers are formed at the early stage of prion replication**

109 The early phases of prion replication are commonly thought to consist of an elongation/growing  
110 process [16], with the PrP<sup>Sc</sup> template serving as a base. We studied the size distribution of  
111 proteinase K (PK)-resistant PrP<sup>Sc</sup> (PrP<sup>res</sup>) assemblies at the early step of prion replication in the  
112 brain by SV in an iodixanol gradient using a previously published methodology [24,49,20]. The  
113 PrP<sup>res</sup> size distribution at the disease end stage served as the control. Three different host  
114 PrP/strain combinations were studied: the 127S cloned scrapie prion strain in ovine PrP tg338  
115 transgenic mice [25], the 139A cloned mouse prion strain in mouse PrP tga20 mice [15] and  
116 the vCJD cloned human prion strain in human PrP tg650 mice [3,19]. As shown in Figure 1A-  
117 C, small oligomers sedimenting between fractions 1 and 4 were preferentially detected at the  
118 early stage of pathogenesis, regardless of the strain considered. A second population of  
119 oligomers with a larger size distribution and peaking in fractions 8-10 and 18 was observed for  
120 127S. At the disease end stage and for the 3 strains, the small assemblies mostly disappeared at  
121 the expense of larger assemblies.

122 To determine whether the formation of small assemblies in the brain at the early stage of  
123 replication can be reproduced by an *in vitro bona fide* amplification method, we used a high-  
124 throughput variant of PMCA (i.e., mb-PMCA), which generates as much infectivity as in the  
125 brain at terminal stage of the disease in one unique round of 48 h, with high reproducibility in  
126 terms of limiting dilution and the amplification yield [31,32]. When the size distribution of the  
127 amplified products was analyzed by SV after one mb-PMCA round, two discrete distributions  
128 were observed for the three strains (Figure 1D). The post-PMCA sedimentograms revealed the  
129 existence of a major set of small PrP<sup>res</sup> assemblies sedimenting between fractions 1 and 3 (peak  
130 P<sub>1</sub>) and a minor set of larger assemblies with a well-defined Gaussian distribution centered on

131 fraction 15 (peak P<sub>2</sub>). The relative proportions of P<sub>1</sub> and P<sub>2</sub> varied among the three strains; P<sub>2</sub>  
132 was barely detected in the 139A amplicons. These data indicate that during mb-PMCA  
133 amplification, two populations of PrP<sup>Sc</sup> assemblies are generated that differ according to their  
134 quaternary structures, with a predominance of small assemblies.

135 The bimodal (i.e., generation of two peaks) and discrete behavior of the size distribution as well  
136 as the formation of predominantly small assemblies in P<sub>1</sub> suggest that the mb-PMCA  
137 condition(s) can be a consequence of shearing forces during the sonication step [1,38,51] rather  
138 than an intrinsic consequence of the replication process. To discriminate between these two  
139 possibilities, undiluted 127S seeds (i.e., 20% brain homogenate) were incubated and sonicated  
140 in identical mb-PMCA conditions but without the PrP<sup>C</sup> substrate (i.e., in PrP<sup>0/0</sup> brain lysate).  
141 As shown in Figure 1E, the size distribution analysis of these sonicated 127S seeds in the PrP<sup>0/0</sup>  
142 substrate revealed mostly the presence of larger-sized assemblies, as observed upon  
143 solubilization at 37°C [24], thus ruling out the mb-PMCA conditions being at the origin of the  
144 formation of small-size assemblies.

145 Altogether, these observations suggest that *in vivo*, the early phase of replication for the 127S,  
146 139A and vCJD prion strains generates mainly small-sized assemblies. Similar to *in vivo*  
147 replication, the mb-PMCA amplification condition generates two sets of PrP assemblies that  
148 differ in their quaternary structures. The formation of these two groups of assemblies is  
149 common to the three strains used here.

150

### 151 P<sub>1</sub> and P<sub>2</sub> contain two structurally distinct PrP<sup>res</sup> assemblies

152 We next asked whether the formation of P<sub>2</sub> resulted from a simple condensation of assemblies  
153 present in the P<sub>1</sub> peak (Oswald ripening process [53]) or from an alternative templating  
154 pathway. To address this question, we first examined the influence of the amplification rate on

155 the formation of these two species by varying the concentration of the seed used as the template  
156 for the mb-PMCA reaction. We compared the SV-sedimentograms of the mb-PMCA products  
157 seeded with  $10^{-3}$  to  $10^{-10}$  diluted 127S brain homogenate. As shown in Figure 2A, as a function  
158 of the seed concentration, the relative amounts of assemblies in P<sub>1</sub> decreased as the amounts of  
159 those from P<sub>2</sub> increased. The variation in the P<sub>1</sub> and P<sub>2</sub> peak surface area as a function of the  
160 logarithm of the dilution factor revealed a quasi-linear decrease in P<sub>1</sub> when the P<sub>2</sub> peak surface  
161 followed a sigmoidal increase (Figure 2B). The sigmoidal increase in P<sub>2</sub> to the detriment of the  
162 quasi-linear decrease in P<sub>1</sub> surface indicates that i) the formation of PrP<sup>res</sup> assemblies present in  
163 P<sub>2</sub> follows a seed concentration-dependent cooperative process and that ii) the formation of the  
164 P<sub>2</sub> peak does not result from the simple condensation of assemblies present in P<sub>1</sub> as the  
165 variations in P<sub>1</sub> and P<sub>2</sub> are uncorrelated (Figure 2B). This observation strongly suggests that  
166 assemblies forming the P<sub>1</sub> and P<sub>2</sub> peaks result from distinct polymerization pathways and should  
167 therefore be structurally distinct.

168 To further explore the entanglement between the assemblies forming P<sub>1</sub> and P<sub>2</sub>, we fixed the  
169 mb-PMCA regime to favor the formation of the P<sub>1</sub> peak by fixing high dilutions of the inoculum  
170 seed, followed by quiescent incubations at 37°C for variable periods. As shown with the 127S  
171 prions, the SV analysis at defined incubation time points post-PMCA reaction revealed a  
172 decrease in the population of P<sub>1</sub> in favor of P<sub>2</sub> (Figure 2C). At 4 h postincubation, there were  
173 equal proportions of assemblies forming P<sub>1</sub> and P<sub>2</sub>. At 24 h, most of the PrP<sup>res</sup> assemblies were  
174 located in the P<sub>2</sub> peak. Comparing the distribution in isopycnic gradients [24] of the PrP<sup>res</sup>  
175 populations at 0h and 24h of quiescent incubation at 37°C revealed a quasi-similar density for  
176 PrP<sup>res</sup> assemblies composing the P<sub>1</sub> and the P<sub>2</sub> peaks (Figure 2D). This observation leads us to  
177 conclude that i) the low sedimentation velocity of the assemblies forming P<sub>1</sub> does not result  
178 from an interaction with lipids or other low-density molecules and ii) the sedimentation velocity

179 increase of P<sub>2</sub> compared to P<sub>1</sub> results strictly from a quaternary structure rearrangement through  
180 size increase rather than change in compactness reducing the hydrodynamic radius.

181 As shown in Figure 2E, the formation of assemblies sedimenting in P<sub>2</sub> exhibited bimodal  
182 behavior (i.e., absence of assemblies of intermediate size) without any significant shift in the  
183 P<sub>2</sub> peak position, suggesting that the formation of these assemblies resulted from the association  
184 with a specific number of assemblies present in P<sub>1</sub>. Furthermore, the time-dependent surface  
185 variation in P<sub>1</sub> and P<sub>2</sub> showed a sigmoidal shape, indicating that the assemblies present in P<sub>2</sub>  
186 enhance their own formation according to an autocatalytic process (Figure 2E). Similarly, the  
187 139A and vCJD prions showed a bimodal evolution of P<sub>1</sub> to P<sub>2</sub> during a 24-h quiescent phase  
188 (Figure 2F), arguing in favor of a generic process of transformation.

189 To determine whether the quaternary structure rearrangement accompanying the transformation  
190 of P<sub>1</sub> to P<sub>2</sub> was in concert with a deeper structural rearrangement in the PrP<sup>Sc</sup> assemblies, we  
191 determined the specific infectivity of the P<sub>1</sub> and P<sub>2</sub> assemblies. A 127S-PMCA product was  
192 fractionated at the end of the reaction or after 48 h of quiescent incubation. Pools of fractions  
193 corresponding to the P<sub>1</sub> and P<sub>2</sub> peaks were inoculated into reporter tg338 mice. The specific  
194 infectivity (infectivity per PrP molecule), which is mostly associated to PrP<sup>res</sup> assemblies  
195 [24,49], was calculated from the mean survival time using 127S dose-response curves [49]. As  
196 shown in Figure 2G, the specific infectivity of the P<sub>1</sub> peak assemblies was 50-100-fold higher  
197 than that of the P<sub>2</sub> peak assemblies. This value did not change over a longer period of quiescent  
198 incubation (7 days, Figure 2G).

199 To determine whether the P<sub>2</sub> peak assemblies could further evolve, we extended the quiescent  
200 phase up to 30 days. For the 127S, 139A and vCJD prion strains, the sedimentogram curves at  
201 7 and 30 days showed a translational shift in the P<sub>2</sub> peak to higher fractions, indicative of an  
202 isokinetic increase in their mean average sizes (Figure 3, left curves). The difference in the

203 specific infectivity values of the P<sub>1</sub> and P<sub>2</sub> peak assemblies did not change over a longer period  
204 of quiescent incubation (7 days, Figure 2G, 127S strain). This size translation thus contrasts  
205 with the bimodal phase and highlights a change in the kinetic regime.

206 Collectively, these observations indicate that the P<sub>1</sub> and P<sub>2</sub> peaks contain structurally distinct  
207 sets of PrP<sup>res</sup> assemblies named A<sub>i</sub> and B<sub>i</sub>. The index i indicates their sizes, with A<sub>i</sub> and B<sub>i</sub> being  
208 the major constituents of the P<sub>1</sub> and P<sub>2</sub> peaks, respectively. The formation of the B<sub>i</sub> assemblies  
209 is cooperative and results from a complex kinetic pathway. Upon longer quiescent incubation,  
210 a change in the kinetic regime occurs.

211

### 212 The formation of B<sub>i</sub> from A<sub>i</sub> assemblies requires the presence of PrP<sup>C</sup> during the 213 quiescent phase

214 Our previous studies revealed that only ~30% of the PrP<sup>C</sup> substrate was converted into PrP<sup>Sc</sup>  
215 after a complete round of mb-PMCA [31,32]. To determine whether the remaining 70% still  
216 participated in the transformation of A<sub>i</sub> to B<sub>i</sub> assemblies during the quiescent phase, PMCA  
217 products from the 139A, 127S and vCJD prions were treated with PK to eliminate PrP<sup>C</sup> before  
218 quiescent incubation at 37°C. As shown in Figure 3 (right curves), the amount of B<sub>i</sub> assemblies  
219 generated during the 48-h quiescent incubation was drastically decreased for the three prion  
220 strains in the absence of the PrP<sup>C</sup> substrate. Further quiescent incubation for 7 and 30 days in  
221 the absence of PrP<sup>C</sup> allowed the formation of low amounts of B<sub>i</sub> assemblies for the 127S and  
222 139A prion strains. The fact that the transformation of A<sub>i</sub> to B<sub>i</sub> assemblies is strongly facilitated  
223 by the presence of PrP<sup>C</sup> suggests that B<sub>i</sub> assemblies result from the integration/conversion of  
224 PrP<sup>C</sup> into A<sub>i</sub> assemblies. The appearance of a low amount of B<sub>i</sub> after a long incubation period  
225 without PrP<sup>C</sup> may result from the leakage of monomers from a conformer cosedimenting with  
226 A<sub>i</sub>.

227

## 228 Kinetical scheme describing the transformation of $A_i$ to $B_i$ assemblies

229 To establish a kinetic mechanism and provide a molecular interpretation of the assemblies'  
230 dynamics during the quiescent phase, a number of elementary steps were identified based on  
231 experimental observations and were used as unavoidable constraints [14]. The first constraint  
232 was the existence of two structurally distinct  $\text{PrP}^{\text{Sc}}$  subassemblies, namely,  $A_i$  and  $B_i$ , with  
233 distinct dynamics. Indeed, structurally equivalent assemblies would fail to present a bimodal  
234 size distribution, cooperative seed concentration and kinetic evolution or distinct specific  
235 infectivity. The second constraint was the existence of a detailed balance between the  $\text{PrP}^{\text{Sc}}$   
236 assemblies and their elementary subunit ( $\text{suPrP}$ ), as previously shown [20] making the size  
237 distribution of the  $\text{PrP}^{\text{Sc}}$  assemblies highly dynamic and dependent on the assembly  
238 concentration, as shown in Figure 1E. Indeed, SV analysis of the  $\text{PrP}^{0/0}$  brains lysates seeded  
239 with 30-fold-diluted 127S-infected brains and submitted to PMCA revealed a quaternary  
240 structure rearrangement with a shift in lower molecular weight assemblies according to the  
241 detailed balance:

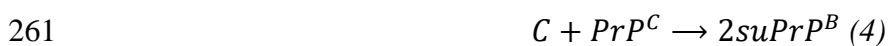


243 where  $\text{PrP}_i^{\text{Sc}}$  and  $\text{PrP}_{i-1}^{\text{Sc}}$  are the sizes  $i$  and  $i-1$  of  $\text{suPrP}^{\text{Sc}}$ , respectively.

244 Because the existence of  $\text{suPrP}$  is a generic property of prion strains [20], the 3<sup>rd</sup> constraint  
245 leads us to assume that the  $A_i$  and  $B_i$  assemblies are in detailed balance with their respective  
246  $\text{suPrPs}$  (denoted  $\text{suPrP}^A$  and  $\text{suPrP}^B$ ) but with distinct equilibrium constants  $K_{eq}^A$  and  $K_{eq}^B$ .  
247 Thus, at any moment of the process of assembly transformation of  $A_i$  to  $B_i$ , the following  
248 equilibrium should be respected:



251 The equilibrium constant  $K_{eq}^{A_i}$  and  $K_{eq}^{B_i}$  governs the respective size distribution of the  $A_i$  and  $B_i$   
252 assemblies and, thus, the bimodal aspect of the curve. According to our previous SV  
253 calibrations with PrP oligomers and globular mass markers [49], the size distribution of the  $A_i$   
254 and  $B_i$  subassemblies were fixed:  $i_A < 5$  and  $i_B$  centered around 20 PrP-mers. Due to the limited  
255 resolution of SV fractionation for small assemblies, we assumed that  $A_i$  and  $suPrP^B$   
256 cosedimented. The fourth constraint relies on the fact that the transformation of A to B requires  
257 PrP<sup>C</sup> and that the kinetic is cooperative, as shown in Figures 1E and 2. This cooperativity  
258 implies that B subassemblies facilitate their own formation according to an autocatalytic  
259 process. This can be resumed by the following minimalistic autocatalytic process:



262 where C is an active complex reacting with PrP<sup>C</sup> that generates B assemblies. Considering that  
263  $suPrP^B$  can condense into  $B_2$  [20] and according to detailed balance (2), one can establish the  
264 reaction model describing the formation of  $B_i$  assemblies from the neo-formed  $suPrP^B$ :



267 Altogether, these six elementary steps constitute the reaction mechanism that describes the  
268 transformation of  $A_i$  into  $B_i$  subassembly species.

269 To validate the designed mechanism, we translated these elementary reactions into time-  
270 dependent differential equations (for more details, see Supplementary text) and performed  
271 kinetic simulations using the size distribution of the PrP<sup>Sc</sup> assemblies immediately after cyclic  
272 amplification as the initial condition (blue curve in Figure 2A). According to the model, the  
273 simulated size distribution variation as a function of time showed bimodal behavior, as was

274 experimentally observed (Figure 4A). Furthermore, the theoretical size distribution centroid  
275 presented similar sigmoidal patterns to those of the experimental data (Figure 4B), arguing in  
276 favor of an autocatalytic kinetic model describing the overall quaternary structure evolution of  
277 PrP<sup>Sc</sup> assemblies during the quiescent phase. The analysis of the model (for more details, see  
278 Supplementary text) revealed that the autocatalytic formation of B<sub>i</sub> species occurs at the  
279 expense of A<sub>i</sub> species and with PrP<sup>C</sup> consumption (Figure 4 C and D). According to this model,  
280 when PrP<sup>C</sup> is in large excess, A<sub>i</sub> constitutes the limiting compound for the formation of B<sub>i</sub>  
281 assemblies. Therefore, during the quiescent phase, the PrP<sup>C</sup> to PrP<sup>Sc</sup> conversion rate is directly  
282 proportional to the amount of A<sub>i</sub> assemblies (Figure 4D).

## 283 Discussion

284 The mechanisms of prion replication and the dynamics responsible for prion structural  
285 diversification in the infected host remain unclear and rarely addressed. In the actual framework  
286 of the prion paradigm, the templating process is admitted to occur at the prion assembly  
287 interface, leading to an increased size of the complex formed by the template:substrate, out of  
288 the fragmentation/depolymerization context. The atypical size distribution observed here at the  
289 early stage of the replication process for three distinct prion strains, where accumulation of  
290 small-size assemblies dominates, contrasts with this canonical templating model and requires  
291 an additional process that considers the dynamics of replication. Furthermore, the existence of  
292 a multistep conversion process provides an unexpected approach to reconciling the best  
293 replicator [35] selection paradigm and diversification process, which is inherent to prion  
294 adaptation and evolution.

295 As shown *in vivo* for the vCJD, 127S and 139A prion strains, the early stage of the replication  
296 process in the brain is dominated by the accumulation of small assemblies, whereas higher-size  
297 subsets are mostly detected at the terminal stage of pathogenesis. Such quaternary structural  
298 diversity, - and beyond the existence of structurally distinct types of assemblies, as defined by  
299 their specific infectivity ([24,49] and Supplemental Figure 1), can be exclusively explained by  
300 the existence of a balance between at least two kinetic modes taking place at different stages of  
301 the pathogenesis. Both can be governed by evolution or a fluctuation in the replication  
302 microenvironment due to the physio-pathological state of the infected animal and/or to the  
303 sequential involvement of specific prion-replicating cell types. However, another possibility  
304 can lie in the intrinsic and deterministic properties of the PrP replication process to generate  
305 structurally distinct types of assemblies. Discriminating between these two nonmutually  
306 exclusive hypotheses is technically difficult *in vivo*. The mb-PMCA as a *bona fide* amplification  
307 method in a more simplified and kinetically controlled context constitutes a relevant method

308 for investigating the intrinsic propensity of the replication process to generate structurally  
309 distinct assemblies. Interestingly, and against common belief, the size distribution of the PrP<sup>Sc</sup>  
310 assemblies used as seeds was relatively insensitive to mb-PMCA sonication cycles when a  
311 simple dilution displaced the assemblies towards a smaller size (Figure 1E), as previously  
312 reported [20]. These two observations exclude the contribution of the fragmentation process  
313 during the mb-PMCA sonication cycles to the size distribution pattern of PrP<sup>Sc</sup> assemblies and  
314 emphasize the existence of a constitutional dynamic between the PrP<sup>Sc</sup> subpopulation [20],  
315 which should be considered during the replication process. We showed that two sets of PrP<sup>Sc</sup>  
316 assemblies, A<sub>i</sub> and B<sub>i</sub>, were generated during the mb-PMCA reaction. The A<sub>i</sub> and B<sub>i</sub> assemblies  
317 constitute two structurally distinct PrP<sup>Sc</sup> subpopulations, as supported by their distinct specific  
318 infectivity; the bimodal size distribution instead of a continuum; the effect of initial seed  
319 concentration on the respective proportions of A<sub>i</sub> and B<sub>i</sub>; and the role of PrP<sup>C</sup> in the  
320 transformation of A<sub>i</sub> to B<sub>i</sub> that indicates that B<sub>i</sub> assemblies do not result from simple  
321 condensation of A<sub>i</sub> assemblies. Therefore, the prion replication process *per se* intrinsically  
322 generates structurally diverse PrP<sup>Sc</sup> subassemblies.

323 According to our SV experiments, small-sized PrP<sup>Sc</sup> assemblies were mainly formed at the early  
324 stage of prion replication in the brain and during the mb-PMCA reaction. This was observed  
325 with three distinct prion strains (127S, 139A, vCJD) on 3 different PrP genetic backgrounds.  
326 Considering that the PrP<sup>Sc</sup> assemblies that constitute each strain are structurally distinct, one  
327 can ask how distinct PrP<sup>Sc</sup> assemblies can all generate A<sub>i</sub> assemblies that harbor strain structural  
328 information while showing the same quaternary structure (at the SV resolution). The first  
329 explanation can be the existence of a common narrow subpopulation of PrP<sup>Sc</sup> (with respect to  
330 their quaternary structure) within the three strains that serves as the best replicator and  
331 participates in the formation of A<sub>i</sub> assemblies. However, the PrP<sup>Sc</sup> quaternary structure subset  
332 that exhibits the highest specific infectivity *in vivo* (i.e., the best replicator) can be associated

333 with either small-size assemblies (i.e., 127S and 139A [24,49] and Supplemental Figure 1A,  
334 respectively) or high-molecular-weight assemblies (i.e., vCJD, Supplemental Figure 1B) and is  
335 therefore strain-dependent. The existence of a structurally common PrP<sup>Sc</sup> subpopulation is thus  
336 unlikely to be at the origin of the generic formation of a small-size subset in the brain or A<sub>i</sub>  
337 assemblies in the mb-PMCA condition. Intrinsically, the early steps of the replication process  
338 favor the emergence of mainly one subspecies A<sub>i</sub> with a highly narrowed size distribution,  
339 arguing in favor of a quaternary structural convergence phenomenon during these steps. This  
340 structural convergence concerns the PrP domain that governs polymerization (the size of  
341 assemblies). However, as the A assemblies harbor the strain structural determinant, one can  
342 conclude that A<sub>i</sub> assemblies present a certain degree of structural variability, allowing the  
343 encoding of strain structural information (Supplemental Figure 1).

344 All along the quiescent phase and for the three prion strains studied, the A<sub>i</sub> assemblies constitute  
345 the precursor species in the formation of B<sub>i</sub> assemblies. Furthermore, the presence of PrP<sup>C</sup> is  
346 required for the evolution of A<sub>i</sub> into B<sub>i</sub> assemblies, and according to the kinetic model  
347 describing the autocatalytic formation of B<sub>i</sub> during the quiescent phase, A<sub>i</sub> is the limiting species  
348 for conversion when large amounts of PrP<sup>C</sup> are present (Figure 4C and D and Supplementary  
349 text). The bimodal quaternary structure evolution during the quiescent phase is in concert with  
350 a specific infectivity decrease that is indicative of a structural rearrangement of species present  
351 in P<sub>1</sub> and P<sub>2</sub> and thus during the transformation of A<sub>i</sub> to B<sub>i</sub>. Even if the first event conducing to  
352 the formation of B<sub>i</sub> assemblies remains undetermined, we can assume that A<sub>i</sub> can have the  
353 intrinsic propensity to spontaneously evolve into B<sub>i</sub> assemblies in the presence of PrP<sup>C</sup> (Figure  
354 5). The cooperative disappearance of P<sub>1</sub> in favor of P<sub>2</sub> strongly suggests an autocatalytic process  
355 for the transformation of A<sub>i</sub> to B<sub>i</sub> (reactions 3 and 4). This last phenomenon shows the existence  
356 of a secondary autocatalytic process, undescribed until now, in the canonical prion replication  
357 process [26]. One can be reasonably envisage that A<sub>i</sub> can have the intrinsic propensity to

358 generate  $B_i$  assemblies in the presence of  $PrP^C$  assemblies with a very low efficiency. This  
359 parallel pathway to the autocatalytic process can then explain how the first set of  $B_i$  assemblies  
360 is generated (Figure 5). The existence of a secondary autocatalytic process can be crucially  
361 important for maintaining  $PrP^{Sc}$  structural diversity throughout the evolution of the pathology.  
362 In the absence of this secondary autocatalytic process, e.g., in the absence of  $PrP^C$ , the system  
363 selects the best replicator and the most thermodynamically stable assemblies. In the presence  
364 of  $PrP^C$ , the system escapes this rule, allowing the specific accumulation of the autocatalytic  
365 product (here, the  $B_i$  assemblies) rather than the assemblies that are the most  
366 thermodynamically stable or have highly specific infectivity. This phenomenon can explain  
367 why, for certain prion strains, the most infectious assemblies represent a minor population,  
368 while those with the lowest specific infectivity mostly accumulate [24,49].

369

## 370 Conclusion

371 The early step of prion replication for at least three distinct prion strains leads to the formation  
372 of small assemblies. The mb-PMCA approach clearly demonstrates the intrinsic properties of  
373 the *bona fide* replication process to generate at least two structurally distinct  $PrP^{Sc}$   
374 subassemblies. The deterministic aspect of the replication process to generate a structurally  
375 diverse set of assemblies contrasts with the widespread idea that considers the prion  
376 diversification process within a given strain (often referred to as the creation of prion quasi-  
377 species) as a stochastic event and as a process that is cogoverned by environmental fluctuations  
378 [52]. The secondary autocatalytic pathway leading to the formation of  $B_i$  subassemblies can  
379 participate in prion adaptation during transmission events with species barriers. Considering  
380 that the transmitted inoculum initially contains  $A_i$  and  $B_i$  assemblies, the autocatalytic  
381 conversion process of  $B_i$  can kinetically drive the adjustment and integration of the new-host

382 PrP<sup>C</sup> to generate host-adapted B<sub>i</sub> assemblies. This hypothesis is supported by our recent  
383 observations in which complementation between A<sub>i</sub> and B<sub>i</sub> subassemblies is required to cross  
384 existing species barriers (submitted article).

385

## 386 **Methods**

### 387 **Ethics**

388 Animal experiments were conducted in strict accordance with ECC and EU directives 86/009  
389 and 2010/63 and were approved by the local ethics committee of the author's institution  
390 (Comethea; permit numbers 12/034 and 15/045).

### 391 **Transgenic mouse lines and prion strains**

392 The ovine (tg338 line; Val136-Arg154-Gln171 VRQ allele), human (tg650 line; Met129 allele)  
393 and mouse (tga20) PrP transgenic lines have been described previously [3,15,25]. The mouse  
394 lines were homozygous and overexpressed approximately 8-, 6-, and 10-fold amounts of  
395 heterologous PrP<sup>C</sup> on a mouse PrP-null background. PrP<sup>0/0</sup> mice were the so-called Zürich-I  
396 mice [10]. Cloned 127S scrapie, human vCJD and mouse 139A prion strains were serially  
397 passaged in tg338, tg650 and tga20 mice, respectively [31,32]. These strains were used as pools  
398 of mouse-infected brains and prepared as 20% wt/vol homogenates in 5% glucose by use of a  
399 tissue homogenizer (Precellys 24 Ribolyzer; Ozyme, France).

### 400 **Time course analysis of prion accumulation**

401 Eight-week-old female tg338, tg650 and tg20 mice were inoculated intracerebrally in the right  
402 cerebral hemisphere with 127S, vCJD or 139A prions (20 µl of a 10% brain homogenate dose).  
403 Infected animals were euthanized by cervical column disruption in triplicate at regular time  
404 points and at the terminal stage of disease. Brains were removed and kept for PrP<sup>Sc</sup> size  
405 fractionation.

#### 406 Miniaturized bead-PMCA assay

407 The miniaturized bead-PMCA assay [11,20,32] was used to amplify prions. Briefly, serial ten-  
408 fold dilutions of 127S, vCJD and 139A prions (mouse brain homogenates diluted in PMCA  
409 buffer) were mixed with brain lysates (10% wt/vol) from healthy tg338, tg650 and tga20 mice  
410 as respective substrates and subjected to one round of 96 cycles of 30-s sonications (220-240  
411 Watts) followed by 29.5 min of incubation at 37°C. With a  $>10^4$  dilution of the seeds, input  
412 PrP<sup>Sc</sup> is not detected in the mb-PMCA products. PMCA was performed in a 96-well microplate  
413 format using a Q700 sonicator (QSonica, USA, Delta Labo, Colombelles, France). For  
414 quiescent incubation, the samples were left in the incubator at 37°C for the indicated period of  
415 time, without any sonication. To eliminate residual PrP<sup>C</sup> present in the PMCA products before  
416 quiescent incubation, the samples were treated with PK (80 µg/ml final concentration). The  
417 treatment was stopped by adding 2 mM Pefabloc and 1x EDTA-free protease inhibitor cocktail.  
418 All final products were kept for PrP<sup>Sc</sup> size fractionation, and aliquots were PK-digested (115  
419 µg/ml final concentration, 0.6% SDS, 1 h, 37°C) prior to immunoblot analyses, as described  
420 below.

#### 421 Sedimentation velocity fractionation

422 SV experiments were performed as described previously [24,49,20]. Mouse brain homogenates  
423 or PMCA products were solubilized by adding an equal volume of solubilization buffer (50  
424 mM HEPES pH 7.4, 300 mM NaCl, 10 mM EDTA, 2 mM DTT, 4% wt/vol dodecyl- β-D-  
425 maltoside (Sigma)) and incubated for 45 min on ice. Sarkosyl (N-lauryl sarcosine; Fluka) was  
426 added to a final concentration of 2% wt/vol, and the incubation continued for an additional 30  
427 min on ice. A total of 150 µl of solubilized samples was loaded atop a 4.8-ml continuous 10–  
428 25% iodixanol gradient (Optiprep, Axys-Shield), with a final concentration of 25 mM HEPES  
429 pH 7.4, 150 mM NaCl, 2 mM EDTA, 1 mM DTT, 0.5% Sarkosyl. The gradients were  
430 centrifuged at 285,000 g for 45 min in a swinging-bucket SW-55 rotor using an Optima LE-

431 80K ultracentrifuge (Beckman Coulter). Gradients were then manually segregated into 30 equal  
432 fractions of 165  $\mu$ l from the bottom using a peristaltic pump and analyzed by immunoblotting  
433 or bioassay for PrP<sup>Sc</sup> or infectivity, respectively. To avoid any cross-contamination, each piece  
434 of equipment was thoroughly decontaminated with 5 M NaOH followed by several rinses in  
435 deionized water after each gradient collection [24].

#### 436 **Isopycnic sedimentation**

437 The entire procedure was performed as described previously [24]. Mouse brain homogenates  
438 or PMCA products were solubilized as described above. For mouse brain homogenates,  
439 solubilization was performed at 37°C to mimic PMCA conditions. A total of 220  $\mu$ l of  
440 solubilized material was mixed to reach 40% iodixanol, 25 mM HEPES pH 7.4, 150 mM NaCl,  
441 2 mM EDTA, 1 mM DTT, 0.5% Sarkosyl final concentration and loaded within a 4.8 ml of 10–  
442 60% discontinuous iodixanol gradient with a final concentration of 25 mM HEPES pH 7.4, 150  
443 mM NaCl, 2 mM EDTA, 1 mM DTT, 0.5% Sarkosyl. The gradients were centrifuged at 115  
444 000 g for 17 hours in a swinging-bucket SW-55 rotor using an Optima LE-80K ultracentrifuge  
445 (Beckman Coulter). Gradients were then manually segregated into 30 equal fractions of 165  $\mu$ l  
446 from the bottom using a peristaltic pump and analyzed for PrP<sup>Sc</sup> content by immunoblotting.

#### 447 **Analysis of PrP<sup>Sc</sup> content by immunoblotting**

448 Aliquots of the SV-fractionated PMCA samples were treated with PK (50  $\mu$ g/ml final  
449 concentration, 1 h, 37°C) before mixing in Laemmli buffer and denaturation at 100°C for 5  
450 min. The samples were run on 12% Bis-Tris Criterion gels (Bio-Rad, Marne la Vallée, France)  
451 and electrotransferred onto nitrocellulose membranes. In some instances, denatured samples  
452 were spotted onto nitrocellulose membranes using a dot-blot apparatus (Schleicher & Schuell  
453 BioScience (Whatman)). Nitrocellulose membranes were probed for PrP with 0.1  $\mu$ g/ml  
454 biotinylated anti-PrP monoclonal antibody Sha31. Immunoreactivity was visualized by  
455 chemiluminescence (GE Healthcare). The protein levels were quantified with ImageLab

456 software after acquisition of chemiluminescent signals with a Chemidoc digital imager (Bio-  
457 Rad, Marnes-la-Coquette, France). For all SDS-PAGE analyses, a fixed quantity of human  
458 recombinant PrP was employed for consistent calibration of the PrP signals in different gels.

### 459 **Bioassays**

460 The pool of fractions of interest was extemporarily diluted ten-fold in 5% glucose and  
461 immediately inoculated via the intracerebral route into reporter tg338 mice (20  $\mu$ l per pool of  
462 fraction, n = 5 mice per pool). Mice showing prion-specific neurological signs were euthanized  
463 at the end stage. To confirm prion disease, brains were removed and analyzed for PrP<sup>Sc</sup> content  
464 using the Bio-Rad TsSeE detection kit [27] prior to immunoblotting, as described above. The  
465 survival time was defined as the number of days from inoculation to euthanasia. To estimate  
466 what the difference in mean survival times means in terms of infectivity, strain-specific curves  
467 correlating the relative infectious dose to survival times were used, as previously described  
468 [49].

### 469 **Kinetic simulation**

470 The details of the kinetic simulation are reported in the Supplementary text. Briefly, two distinct  
471 sets of assemblies were considered ( $A_i$  and  $B_i$ ). Based on experimental observations, a set of  
472 constraints was retained to build biochemical reactions describing the evolution of the  
473 quaternary structure of PrP<sup>res</sup> assemblies. The ordinary differential equations of the biochemical  
474 reactions 1 to 6 (in the manuscript) were established and coded in MATLAB for simulations.

## 475 **Legends**

### 476 **Figure 1. Size distribution of PrP<sup>Sc</sup> assemblies from different prion strains at the early** 477 **and late stages of pathogenesis *in vivo* and after the PMCA reaction**

478 The size distribution of proteinase K (PK)-resistant PrP<sup>Sc</sup> assemblies present in the brain *in vivo*  
479 (A-C) and in PMCA products (D-E) was examined by sedimentation velocity (SV).

480 (A-C) For the *in vivo* sedimentograms, brains from ovine (tg338), murine (tga20) and human  
481 (tg650) transgenic mice inoculated with 127S scrapie prions (A), 139A mouse prions (B) and  
482 vCJD human prions (C) were collected (in triplicate) at the early stage (15 days postinfection  
483 (127S), 11 days postinfection (139A) and 120 days postinfection (vCJD), blue curves) and at  
484 the end stage of the disease (60 days postinfection (127S), 55 days postinfection (139A), 495  
485 days postinfection (vCJD), red curves). The brains were solubilized and SV-fractionated. The  
486 collected fractions (numbered from top to bottom) were analyzed for PK-resistant PrP<sup>Sc</sup> content  
487 by immunoblotting.

488 (D-E) For the sedimentograms from the PMCA products with PrP<sup>C</sup> substrate (D), the same  
489 strains were subjected to a single round of mb-PMCA by using 10<sup>-5</sup> (139A) or 10<sup>-6</sup> (vCJD,  
490 127S) diluted brain homogenates as seed for the reaction. Thirty minutes after the last  
491 sonication, the amplified products were solubilized and SV-fractionated. The mean levels of  
492 PK-resistant PrP<sup>Sc</sup> per fraction were obtained from the immunoblot analysis of  $n=4$  independent  
493 fractionations of PMCA reactions. The peaks containing PrP<sup>Sc</sup> assemblies sedimentating in the  
494 top and middle fractions were termed P<sub>1</sub> and P<sub>2</sub>, respectively. For the sedimentograms from the  
495 PMCA products without PrP<sup>C</sup> substrate (E), undiluted 127S-infected tg338 brain (20% w/v, red  
496 curve) or a 1:32 dilution in PMCA buffer (blue curve) was used as seed, mixed with brain  
497 homogenate from PrP<sup>0/0</sup> mice as substrate and subjected to a single round of mb-PMCA before  
498 SV fractionation (mean levels from  $n=3$  independent fractionations).

499

500 **Figure 2. Seed concentration- and time-dependent dynamic evolution of the PMCA-**  
501 **generated PrP<sup>Sc</sup> assemblies**

502 **(A-B)** SV profile of mb-PMCA products seeded with ten-fold dilutions from 127S-infected  
503 brain homogenates, as indicated. Thirty minutes after the last sonication, the amplified products  
504 were solubilized and SV-fractionated. The mean relative levels of PK-resistant PrP<sup>Sc</sup> per  
505 fraction **(A)** were obtained from the immunoblot analysis of  $n=4$  independent fractionations of  
506 PMCA reactions (representative dot-blot shown). Variation in the P<sub>1</sub> and P<sub>2</sub> peak surface areas  
507 as a function of the logarithm of the seed dilution factor **(B)**.

508 **(C)** PK-resistant PrP<sup>Sc</sup> sedimentograms from the PMCA products generated with 127S prions  
509 ( $10^{-5}$  dilution) and further incubated at 37°C during the indicated quiescent phase ( $t$ ), i.e.,  
510 without sonication. At each time point, the collected products were frozen. All collected  
511 samples were then thawed, fractionated in parallel by SV and analyzed by immunoblot **(C,  $n=3$ )**  
512 independent experiments, representative dot-blot shown).

513 **(D)** PK-resistant PrP<sup>Sc</sup> isopycnic sedimentograms from PMCA products generated with 127S  
514 prions ( $10^{-5}$  dilution) and immediately fractionated at the end of the PMCA reaction (blue line  
515 and symbol) or after a 24h-quiescent incubation at 37°C (red line and symbol). At each time  
516 point, the collected samples were frozen. All collected samples were then thawed, fractionated  
517 in parallel by sedimentation at the equilibrium [24] and analyzed by immunoblot (the mean  
518 levels of PK-resistant PrP<sup>Sc</sup> per fraction were obtained from the immunoblot analysis of  $n=3$   
519 independent fractionations of PMCA reactions). As control, the density profile of PK-resistant  
520 PrP<sup>Sc</sup> assemblies from the brain of terminally sick tg338 mice (solubilization at 37°C to mimic  
521 the PMCA conditions) is shown (gray line and symbol).

522 **(E)** Evolution of the percentage of P<sub>1</sub> and P<sub>2</sub> peaks as a function of the quiescent phase post-  
523 PMCA reaction **(C)**.

524 (F) PK-resistant PrP<sup>Sc</sup> sedimentograms from the PMCA products generated with 139A and  
525 vCJD prion seeds ( $10^{-5}$  dilution) and further incubated for a quiescent period of 24 h at 37°C.  
526 (G) Specific infectivity of the P<sub>1</sub> and P<sub>2</sub> peaks post-PMCA reaction and after quiescent  
527 incubation. Fractions corresponding to P<sub>1</sub> (fractions 1-3) and P<sub>2</sub> (fractions 14-16 (days 0 and 2)  
528 or 16-18 (day 7)) were pooled and inoculated into groups of reporter tg338 mice at two different  
529 dilutions (1:10 and 1:1000) for better accuracy. The specific infectivity of the assemblies was  
530 calculated from the mean survival time of the mice using a 127S dose-response curve. \*:  
531 incomplete attack rate.

532

### 533 **Figure 3. PrP-dependent generation of B<sub>i</sub> assemblies from A<sub>i</sub> assemblies**

534 PMCA products from 127S, 139A and vCJD prions ( $10^5$ ,  $10^4$  and  $10^4$  diluted seeds,  
535 respectively) were treated with or without PK to eliminate PrP<sup>C</sup> before quiescent incubation at  
536 37°C for 24 h, 7 days or 30 days, as indicated. At each time point, the collected products were  
537 frozen. All collected samples were then thawed, SV-fractionated in parallel and analyzed by  
538 immunoblotting ( $n=3$  independent experiments).

539

### 540 **Figure 4. Mathematical modeling of the time-dependent dynamic evolution of the PMCA-** 541 **generated PrP<sup>Sc</sup> assemblies**

542 (A) The size distribution evolution of a structurally distinct set of assemblies A<sub>i</sub> and B<sub>i</sub>  
543 dimensioned on gradient fraction numbers was simulated based on the kinetic scheme described  
544 in the results section (equations 1 to 6) and the Supplementary text.

545 (B) The time dependency evolution of the simulated centroid (black line) and centroid  
546 calculated from experimental sedimentograms of Figure 2D (red circle) show a similar shape,  
547 supporting the cooperativity hypothesis of the transformation of A<sub>i</sub> into B<sub>i</sub>.

548 (C) The simulation of time dependency evolution of the total amount of  $A_i$  assemblies ( $\sum iA_i$   
549 in black),  $B_i$  assemblies ( $\sum iB_i$  in blue) and the monomer (in red) revealed that  $A_i$  assemblies  
550 constitute the limiting species for the conversion of  $\text{PrP}^C$  during the quiescent phase. In the  
551 present simulation framework (for more details, see Supplementary text), only 14% of  $\text{PrP}^C$  is  
552 consumed.

553

554 **Figure 5. Quaternary structural convergence and secondary autocatalytic pathway at the**  
555 **root of the formation of  $B_i$  assemblies**

556 (A) Different prion strains ( $S_1$ ,  $S_2$  and  $S_3$ ) give rise to the formation of common oligomeric  
557 assemblies, termed  $A_i$ , with a narrowed size distribution during mb-PMCA reactions. This  
558 common quaternary structural convergence at the early stage of the replication process suggests  
559 the existence of a common conversion pathway and a common oligomerization domain that is  
560 independent of the strain structural determinant (SSD, represented in red).

561 (B) According to the dilution experiments (see Figure 1E), an equilibrium exists between  $\text{PrP}^{\text{Sc}}$   
562 assemblies and the suPrP from each subpopulation [20]. Based on the constraints imposed by  
563 the experimental observations, the best model to account for the cooperative and  $\text{PrP}^C$   
564 dependency transformation of  $A_i$  into  $B_i$  assemblies implicates a secondary templating pathway  
565 where the transformation of suPrP<sup>A</sup> to suPrP<sup>B</sup> is assisted by suPrP<sup>B</sup>, rendering the process  
566 autocatalytic.

567

568 **Supplemental Figure 1. PK-resistant  $\text{PrP}^{\text{Sc}}$  and the infectivity sedimentation profile of**  
569 **139A and vCJD prion strains**

570 Brain homogenates from tga20 mice infected with 139A prions (A) and tg650 mice infected  
571 with vCJD prions (B) were solubilized and SV-fractionated. The collected fractions were  
572 analyzed for PK-resistant  $\text{PrP}^{\text{Sc}}$  content (black line) and for infectivity (red bars or line) with an

573 incubation time bioassay in reporter tga20 and tg650 mice. The mean survival time values of  
574 these mice were reported as standard dose-response curves ([18] and unpublished) to determine  
575 relative infectious dose values. A relative infectious dose of 0 corresponds to animals inoculated  
576 with 2 mg of infectious brain tissue.  
577

## 578 **References**

- 579 1. Adachi M, So M, Sakurai K, Kardos J, Goto Y (2015) Supersaturation-limited and Unlimited  
580 Phase Transitions Compete to Produce the Pathway Complexity in Amyloid  
581 Fibrillation. *J Biol Chem* 290:18134-18145. doi:10.1074/jbc.M115.648139
- 582 2. Angers RC, Kang HE, Napier D, Browning S, Seward T, Mathiason C, Balachandran A,  
583 McKenzie D, Castilla J, Soto C, Jewell J, Graham C, Hoover EA, Telling GC (2010)  
584 Prion strain mutation determined by prion protein conformational compatibility and  
585 primary structure. *Science* 328:1154-1158. doi:10.1126/science.1187107
- 586 3. Beringue V, Le Dur A, Tixador P, Reine F, Lepourry L, Perret-Liaudet A, Haik S, Vilotte  
587 JL, Fontes M, Laude H (2008) Prominent and persistent extraneural infection in human  
588 PrP transgenic mice infected with variant CJD. *PLoS One* 3:e1419.  
589 doi:10.1371/journal.pone.0001419
- 590 4. Beringue V, Vilotte JL, Laude H (2008) Prion agent diversity and species barrier. *Vet Res*  
591 39:47. doi:10.1051/vetres:2008024  
592 v08241 [pii]
- 593 5. Bessen RA, Marsh RF (1994) Distinct PrP properties suggest the molecular basis of strain  
594 variation in transmissible mink encephalopathy. *J Virol* 68:7859-7868
- 595 6. Bett C, Joshi-Barr S, Lucero M, Trejo M, Liberski P, Kelly JW, Masliah E, Sigurdson CJ  
596 (2012) Biochemical properties of highly neuroinvasive prion strains. *PLoS Pathog*  
597 8:e1002522. doi:10.1371/journal.ppat.1002522  
598 PPATHOGENS-D-11-02044 [pii]
- 599 7. Bett C, Lawrence J, Kurt TD, Orru C, Aguilar-Calvo P, Kincaid AE, Surewicz WK, Caughey  
600 B, Wu C, Sigurdson CJ (2017) Enhanced neuroinvasion by smaller, soluble prions. *Acta*  
601 *Neuropathol Commun* 5:32. doi:10.1186/s40478-017-0430-z
- 602 8. Bruce ME (2003) TSE strain variation. *Br Med Bull* 66:99-108

- 603 9. Brundin P, Melki R, Kopito R (2010) Prion-like transmission of protein aggregates in  
604 neurodegenerative diseases. *Nat Rev Mol Cell Biol* 11:301-307. doi:10.1038/nrm2873
- 605 10. Bueler H, Fischer M, Lang Y, Bluethmann H, Lipp HP, DeArmond SJ, Prusiner SB, Aguet  
606 M, Weissmann C (1992) Normal development and behaviour of mice lacking the  
607 neuronal cell-surface PrP protein. *Nature* 356:577-582. doi:10.1038/356577a0
- 608 11. Chapuis J, Moudjou M, Reine F, Herzog L, Jaumain E, Chapuis C, Quadrio I, Boulliat J,  
609 Perret-Liaudet A, Dron M, Laude H, Rezaei H, Beringue V (2016) Emergence of two  
610 prion subtypes in ovine PrP transgenic mice infected with human MM2-cortical  
611 Creutzfeldt-Jakob disease prions. *Acta neuropathologica communications* 4:2-15.  
612 doi:10.1186/s40478-016-0284-9
- 613 12. Collinge J, Clarke AR (2007) A general model of prion strains and their pathogenicity.  
614 *Science* 318:930-936
- 615 13. Condello C, Stohr J (2017) Abeta propagation and strains: Implications for the phenotypic  
616 diversity in Alzheimer's disease. *Neurobiol Dis.* doi:10.1016/j.nbd.2017.03.014
- 617 14. Epstein IR, Pojman JA (1998) An introduction to nonlinear chemical dynamics:  
618 oscillations, waves, patterns and chaos. Oxford University Press, Oxford
- 619 15. Fischer M, Rulicke T, Raeber A, Sailer A, Moser M, Oesch B, Brandner S, Aguzzi A,  
620 Weissmann C (1996) Prion protein (PrP) with amino-proximal deletions restoring  
621 susceptibility of PrP knockout mice to scrapie. *EMBO J* 15:1255-1264
- 622 16. Gaspar R, Meisl G, Buell AK, Young L, Kaminski CF, Knowles TPJ, Sparr E, Linse S  
623 (2017) Secondary nucleation of monomers on fibril surface dominates alpha-synuclein  
624 aggregation and provides autocatalytic amyloid amplification. *Q Rev Biophys* 50:e6.  
625 doi:10.1017/S0033583516000172
- 626 17. Griffith JS (1967) Self-replication and scrapie. *Nature* 215:1043-1044

- 627 18. Halliez S, Reine F, Herzog L, Jaumain E, Haik S, Rezaei H, Vilotte JL, Laude H, Beringue  
628 V (2014) Accelerated, spleen-based titration of variant Creutzfeldt-Jakob disease  
629 infectivity in transgenic mice expressing human prion protein with sensitivity  
630 comparable to that of survival time bioassay. *J Virol* 88:8678-8686.  
631 doi:10.1128/JVI.01118-14
- 632 19. Halliez S, Reine F, Herzog L, Jaumain E, Haik S, Rezaei H, Vilotte JL, Laude H, Beringue  
633 V (2014) Accelerated, spleen-based titration of variant Creutzfeldt-Jakob disease  
634 infectivity in transgenic mice expressing human prion protein with sensitivity  
635 comparable to that of survival time bioassay. *Journal of Virology* 88:8678-8686.  
636 doi:10.1128/jvi.01118-14
- 637 20. Igel-Egalon A, Moudjou M, Martin D, Busley A, Knapple T, Herzog L, Reine F, Lepejova  
638 N, Richard CA, Beringue V, Rezaei H (2017) Reversible unfolding of infectious prion  
639 assemblies reveals the existence of an oligomeric elementary brick. *PLoS Pathog*  
640 13:e1006557. doi:10.1371/journal.ppat.1006557
- 641 21. Jucker M, Walker LC (2011) Pathogenic protein seeding in Alzheimer disease and other  
642 neurodegenerative disorders. *Ann Neurol* 70:532-540. doi:10.1002/ana.22615
- 643 22. Jucker M, Walker LC (2013) Self-propagation of pathogenic protein aggregates in  
644 neurodegenerative diseases. *Nature* 501:45-51. doi:10.1038/nature12481
- 645 23. Kim C, Haldiman T, Surewicz K, Cohen Y, Chen W, Blevins J, Sy MS, Cohen M, Kong  
646 Q, Telling GC, Surewicz WK, Safar JG (2012) Small Protease Sensitive Oligomers of  
647 PrP(Sc) in Distinct Human Prions Determine Conversion Rate of PrP(C). *PLoS Pathog*  
648 8:e1002835. doi:10.1371/journal.ppat.1002835
- 649 PPATHOGENS-D-12-00720 [pii]
- 650 24. Laferriere F, Tixador P, Moudjou M, Chapuis J, Sibille P, Herzog L, Reine F, Jaumain E,  
651 Laude H, Rezaei H, Beringue V (2013) Quaternary structure of pathological prion

- 652 protein as a determining factor of strain-specific prion replication dynamics. *PLoS*  
653 *Pathog* 9:e1003702. doi:10.1371/journal.ppat.1003702
- 654 PPATHOGENS-D-13-00529 [pii]
- 655 25. Langevin C, Andreoletti O, Le Dur A, Laude H, Beringue V (2011) Marked influence of  
656 the route of infection on prion strain apparent phenotype in a scrapie transgenic mouse  
657 model. *Neurobiol Dis* 41:219-225. doi:S0969-9961(10)00311-6 [pii]  
658 10.1016/j.nbd.2010.09.010
- 659 26. Lansbury PT, Jr., Caughey B (1995) The chemistry of scrapie infection: implications of the  
660 'ice 9' metaphor. *Chem Biol* 2:1-5
- 661 27. Le Dur A, Beringue V, Andreoletti O, Reine F, Lai TL, Baron T, Bratberg B, Vilotte JL,  
662 Sarradin P, Benestad SL, Laude H (2005) A newly identified type of scrapie agent can  
663 naturally infect sheep with resistant PrP genotypes. *Proc Natl Acad Sci U S A*  
664 102:16031-16036. doi:0502296102 [pii]  
665 10.1073/pnas.0502296102
- 666 28. Le Dur A, Lai TL, Stinnakre MG, Laisne A, Chenais N, Rakotobe S, Passet B, Reine F,  
667 Soulier S, Herzog L, Tilly G, Rezaei H, Beringue V, Vilotte JL, Laude H (2017)  
668 Divergent prion strain evolution driven by PrPC expression level in transgenic mice.  
669 *Nat Commun* 8:14170. doi:10.1038/ncomms14170
- 670 29. Li J, Browning S, Mahal SP, Oelschlegel AM, Weissmann C (2010) Darwinian evolution  
671 of prions in cell culture. *Science* 327:869-872. doi:10.1126/science.1183218
- 672 30. Masel J, Jansen VA, Nowak MA (1999) Quantifying the kinetic parameters of prion  
673 replication. *Biophys Chem* 77:139-152
- 674 31. Moudjou M, Chapuis J, Mekrouti M, Reine F, Herzog L, Sibille P, Laude H, Vilette D,  
675 Andreoletti O, Rezaei H, Dron M, Beringue V (2016) Glycoform-independent prion

- 676 conversion by highly efficient, cell-based, protein misfolding cyclic amplification. *Sci*  
677 *Rep* 6:29116. doi:10.1038/srep29116
- 678 32. Moudjou M, Sibille P, Fichet G, Reine F, Chapuis J, Herzog L, Jaumain E, Laferriere F,  
679 Richard CA, Laude H, Andreoletti O, Rezaei H, Beringue V (2014) Highly infectious  
680 prions generated by a single round of microplate-based protein misfolding cyclic  
681 amplification. *MBio* 5:e00829-00813. doi:10.1128/mBio.00829-13
- 682 33. Moulin E, Giuseppone N (2012) Dynamic combinatorial self-replicating systems. *Top Curr*  
683 *Chem* 322:87-105. doi:10.1007/128\_2011\_198
- 684 34. Nakaoka R, Sakaguchi S, Atarashi R, Nishida N, Arima K, Shigematsu K, Katamine S  
685 (2000) Early appearance but lagged accumulation of detergent-insoluble prion protein  
686 in the brains of mice inoculated with a mouse-adapted Creutzfeldt-Jakob disease agent.  
687 *Cell Mol Neurobiol* 20:717-730
- 688 35. Nee S (2016) The evolutionary ecology of molecular replicators. *R Soc Open Sci* 3:160235.  
689 doi:10.1098/rsos.160235
- 690 36. Ohhashi Y, Yamaguchi Y, Kurahashi H, Kamatari YO, Sugiyama S, Uluca B, Piechatzek  
691 T, Komi Y, Shida T, Muller H, Hanashima S, Heise H, Kuwata K, Tanaka M (2018)  
692 Molecular basis for diversification of yeast prion strain conformation. *Proc Natl Acad*  
693 *Sci U S A* 115:2389-2394. doi:10.1073/pnas.1715483115
- 694 37. Ojosnegros S, Perales C, Mas A, Domingo E (2011) Quasispecies as a matter of fact: viruses  
695 and beyond. *Virus Res* 162:203-215. doi:10.1016/j.virusres.2011.09.018
- 696 38. Okumura H, Itoh SG (2014) Amyloid fibril disruption by ultrasonic cavitation:  
697 nonequilibrium molecular dynamics simulations. *J Am Chem Soc* 136:10549-10552.  
698 doi:10.1021/ja502749f
- 699 39. Prusiner SB (1982) Novel proteinaceous infectious particles cause scrapie. *Science*  
700 216:136-144

- 701 40. Saborio GP, Permanne B, Soto C (2001) Sensitive detection of pathological prion protein  
702 by cyclic amplification of protein misfolding. *Nature* 411:810-813.  
703 doi:10.1038/35081095
- 704 41. Sajnani G, Silva CJ, Ramos A, Pastrana MA, Onisko BC, Erickson ML, Antaki EM, Dynin  
705 I, Vazquez-Fernandez E, Sigurdson CJ, Carter JM, Requena JR (2012) PK-sensitive PrP  
706 is infectious and shares basic structural features with PK-resistant PrP. *PLoS Pathog*  
707 8:e1002547. doi:10.1371/journal.ppat.1002547
- 708 PPATHOGENS-D-11-01621 [pii]
- 709 42. Sandberg MK, Al-Doujaily H, Sharps B, Clarke AR, Collinge J (2011) Prion propagation  
710 and toxicity in vivo occur in two distinct mechanistic phases. *Nature* 470:540-542.  
711 doi:10.1038/nature09768
- 712 43. Sandberg MK, Al-Doujaily H, Sharps B, De Oliveira MW, Schmidt C, Richard-Londt A,  
713 Lyall S, Linehan JM, Brandner S, Wadsworth JD, Clarke AR, Collinge J (2014) Prion  
714 neuropathology follows the accumulation of alternate prion protein isoforms after  
715 infective titre has peaked. *Nat Commun* 5:4347. doi:10.1038/ncomms5347
- 716 44. Silveira JR, Raymond GJ, Hughson AG, Race RE, Sim VL, Hayes SF, Caughey B (2005)  
717 The most infectious prion protein particles. *Nature* 437:257-261. doi:nature03989 [pii]  
718 10.1038/nature03989
- 719 45. Sim VL, Caughey B (2009) Ultrastructures and strain comparison of under-glycosylated  
720 scrapie prion fibrils. *Neurobiol Aging* 30:2031-2042.  
721 doi:10.1016/j.neurobiolaging.2008.02.016
- 722 46. Simoneau S, Rezaei H, Sales N, Kaiser-Schulz G, Lefebvre-Roque M, Vidal C, Fournier  
723 JG, Comte J, Wopfner F, Grosclaude J, Schatzl H, Lasmezas CI (2007) In vitro and in  
724 vivo neurotoxicity of prion protein oligomers. *PLoS Pathog* 3:e125.  
725 doi:10.1371/journal.ppat.0030125

- 726 47. Spassov S, Beekes M, Naumann D (2006) Structural differences between TSEs strains  
727 investigated by FT-IR spectroscopy. *Biochim Biophys Acta* 1760:1138-1149.  
728 doi:S0304-4165(06)00042-0 [pii]  
729 10.1016/j.bbagen.2006.02.018
- 730 48. Telling GC, Parchi P, DeArmond SJ, Cortelli P, Montagna P, Gabizon R, Mastrianni J,  
731 Lugaresi E, Gambetti P, Prusiner SB (1996) Evidence for the conformation of the  
732 pathologic isoform of the prion protein enciphering and propagating prion diversity.  
733 *Science* 274:2079-2082
- 734 49. Tixador P, Herzog L, Reine F, Jaumain E, Chapuis J, Le Dur A, Laude H, Beringue V  
735 (2010) The physical relationship between infectivity and prion protein aggregates is  
736 strain-dependent. *PLoS Pathog* 6:e1000859. doi:10.1371/journal.ppat.1000859
- 737 50. Tzaban S, Friedlander G, Schonberger O, Horonchik L, Yedidia Y, Shaked G, Gabizon R,  
738 Taraboulos A (2002) Protease-sensitive scrapie prion protein in aggregates of  
739 heterogeneous sizes. *Biochemistry* 41:12868-12875. doi:bi025958g [pii]
- 740 51. Webster GT, Dusting J, Balabani S, Blanch EW (2011) Detecting the early onset of shear-  
741 induced fibril formation of insulin in situ. *J Phys Chem B* 115:2617-2626.  
742 doi:10.1021/jp110367t
- 743 52. Weissmann C, Li J, Mahal SP, Browning S (2011) Prions on the move. *EMBO Rep*  
744 12:1109-1117. doi:embor2011192 [pii]  
745 10.1038/embor.2011.192
- 746 53. Zhang J, Muthukumar M (2009) Simulations of nucleation and elongation of amyloid  
747 fibrils. *J Chem Phys* 130:035102. doi:10.1063/1.3050295
- 748

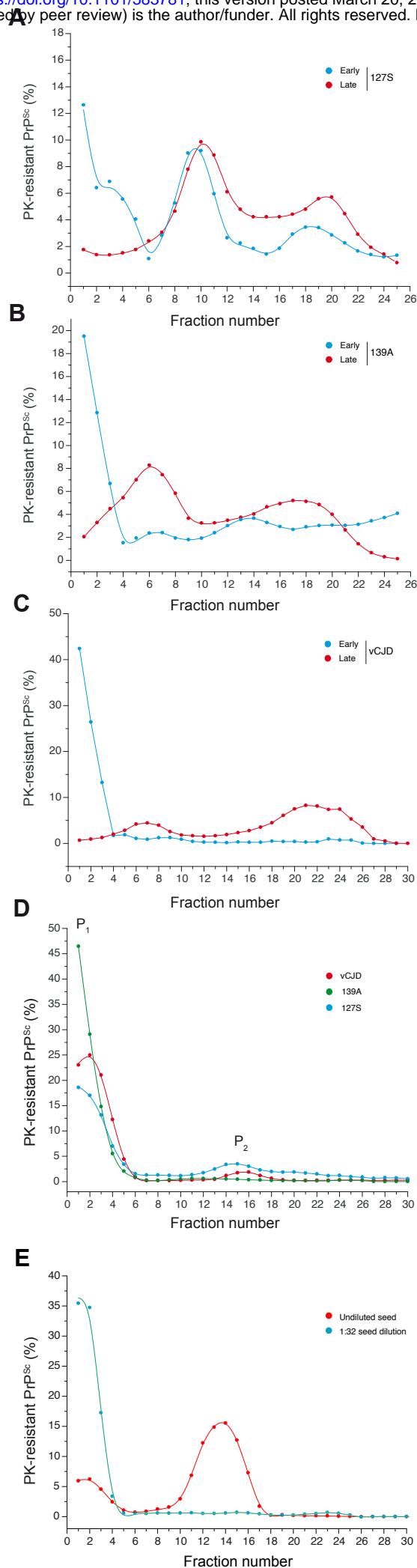


Figure 1

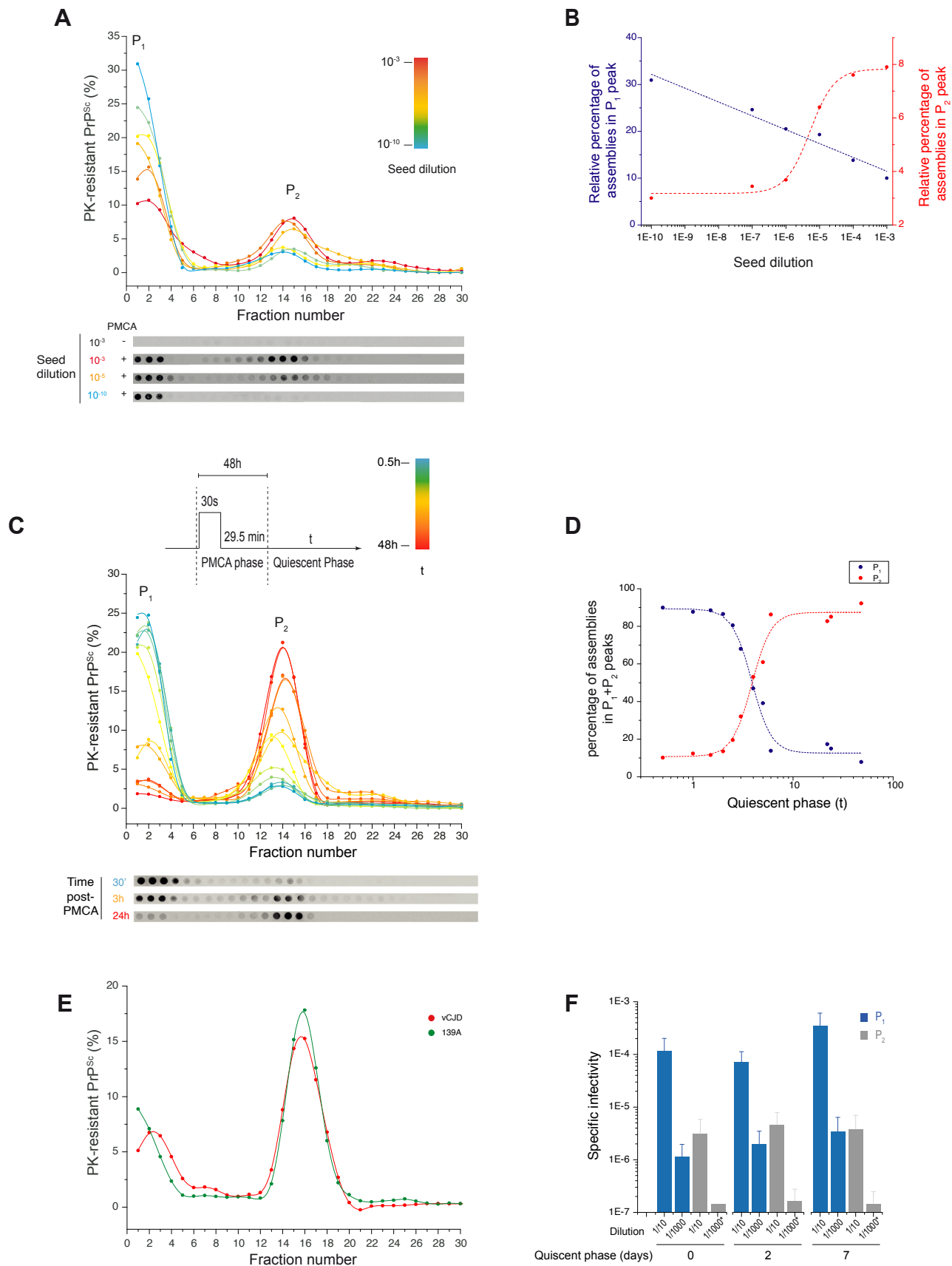
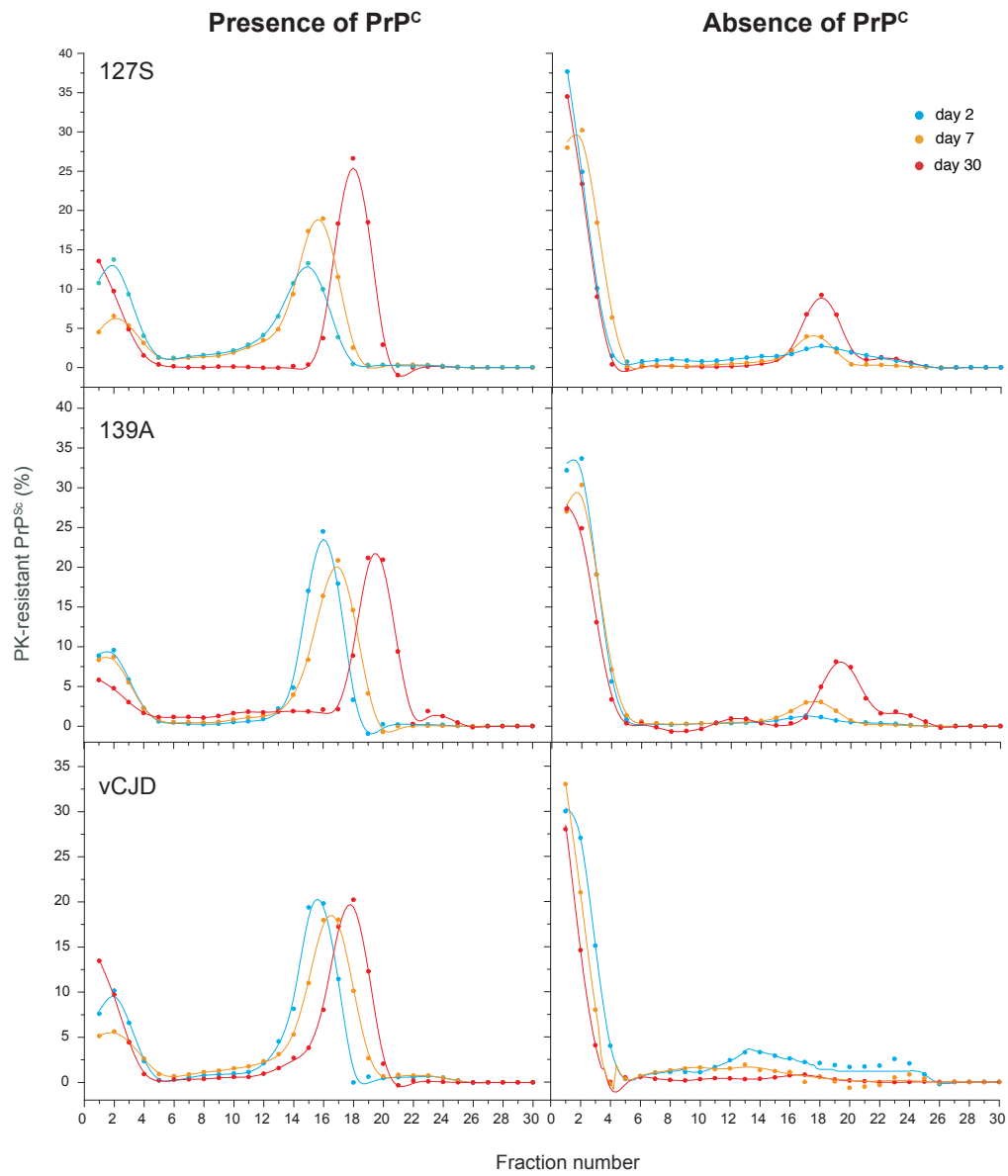
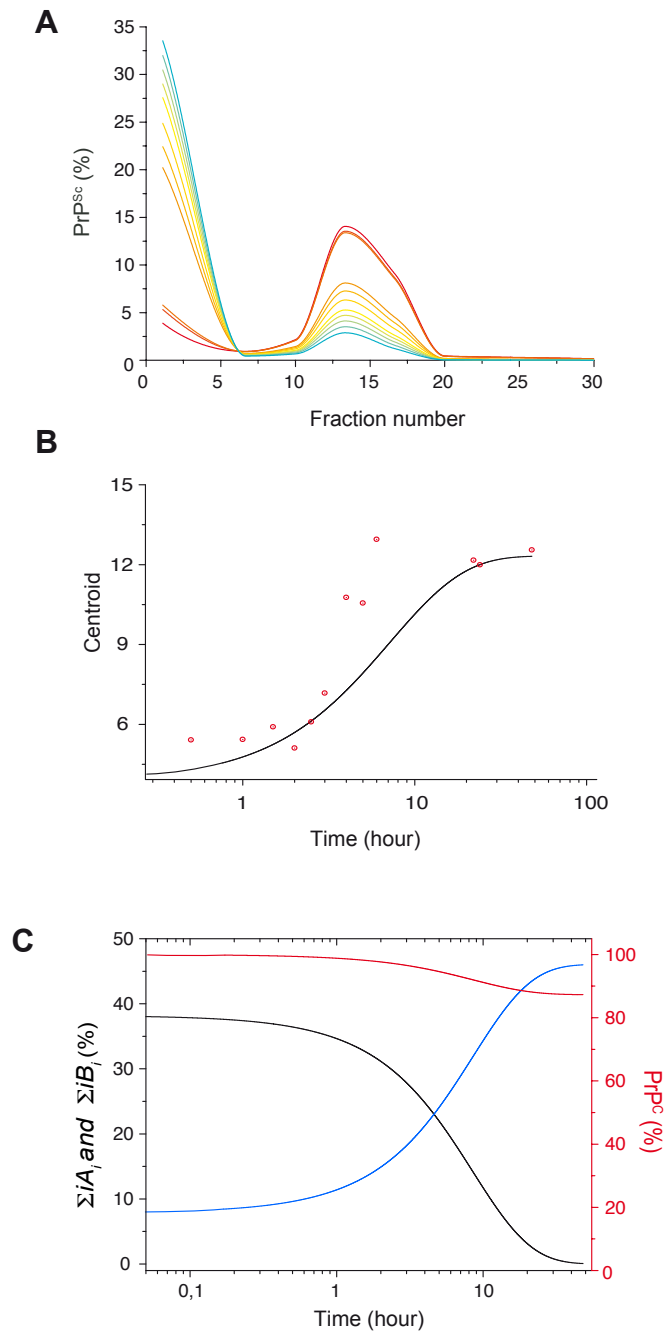


Figure 2



**Figure 3**



**Figure 4**

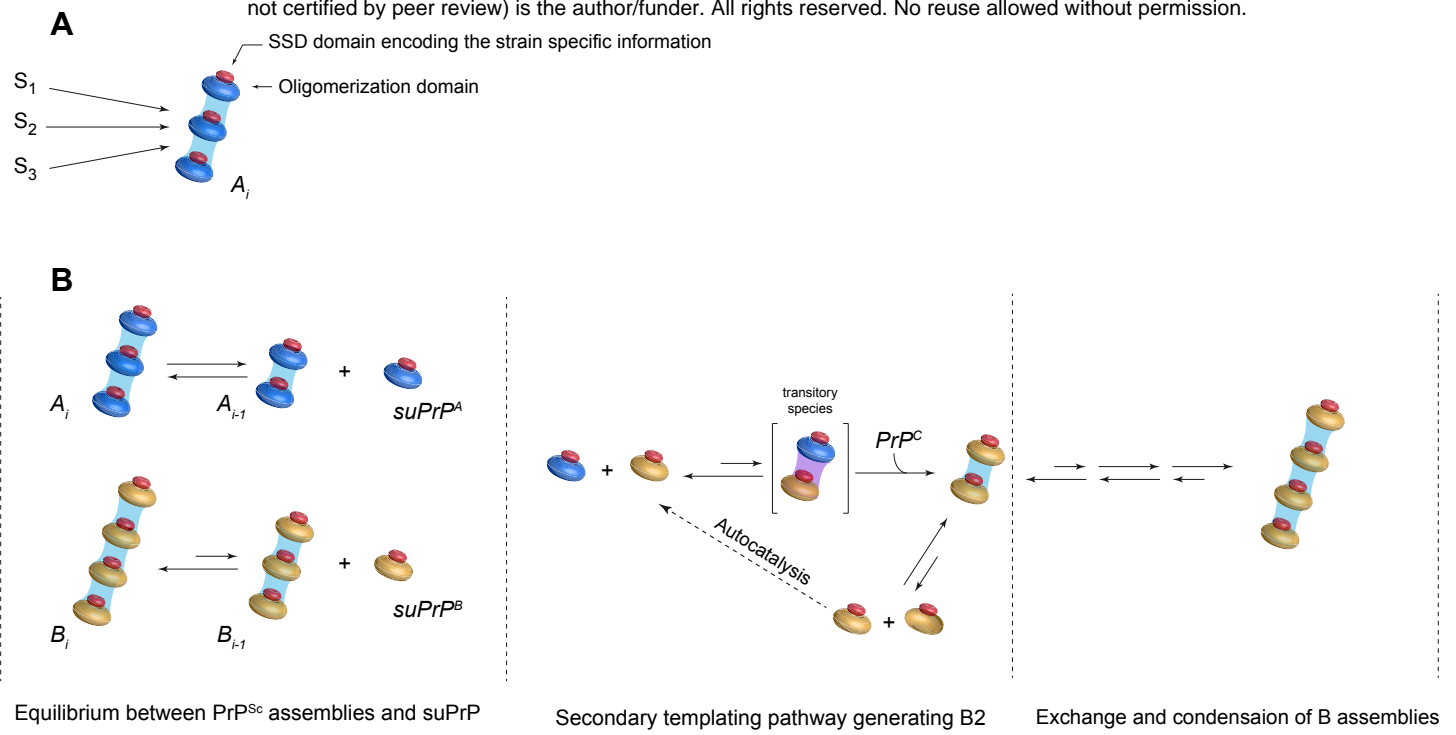


Figure 5